Available online at www.sciencedirect.com
SCIENCE DIRECT®
Journal of Solid State Chemistry 178 (2005) 3672–3678
JOURNAL OF SOLID STATE CHEMISTRY
www.elsevier.com/locate/jssc

Dehydrogenation kinetics of as-received and ball-milled $LiAlH_4$

A. Andreasen[a,b,*,1], T. Vegge[a], A.S. Pedersen[a]

[a]*Materials Research Department, Risø National Laboratory, DK-4000 Roskilde, Denmark*
[b]*Interdisciplinary Research Center for Catalysis, Department of Chemical Engineering, Technical University of Denmark, DK-2800 Lyngby, Denmark*

Received 21 June 2005; received in revised form 14 September 2005; accepted 14 September 2005
Available online 19 October 2005

Abstract

In this paper, we investigate the dehydrogenation kinetics of $LiAlH_4$ into Li_3AlH_6 (reaction I) and further into LiH (reaction II). We find the apparent activation energies to be ~80 and 100 kJ/mol for reactions I and II, respectively. Furthermore, we investigate the effect of ball milling on crystallite size and the dehydrogenation kinetics of both reactions I and II. We find a clear correlation between crystallite size and dehydrogenation kinetics of reaction I. On the other hand, we find the kinetics of reaction II to be independent of the crystallite size. This indicates that reaction I is limited by a mass transfer process, while reaction II is limited by the intrinsic kinetics.
© 2005 Elsevier Inc. All rights reserved.

Keywords: Hydrogen storage materials; Ball milling; X-ray diffraction; Lithium tetrahydroaluminate; Trilithium hexahydroaluminate; Gravimetry; Dehydrogenation kinetics

1. Introduction

The energy infrastructure is facing serious challenges in the future, due to limited supply of oil, increasing CO_2 emissions, and an expansive energy demand in the growing Asian economies.

Hydrogen is a potential major alternative energy carrier, although a smooth transition to a hydrogen-based society requires a solution to several technical problems; especially the need for a proper hydrogen storage medium for the transport sector is a great challenge [1,2].

Until recently, complex hydrides such as $NaAlH_4$ and $LiAlH_4$, with a theoretical capacity of 7.3 and 10.6 wt% H_2, respectively, have not been considered as potential solid state hydrogen storage media due to their irreversible dehydrogenation and slow kinetics. This perception did not change until the 1997 discovery of Ti-catalysed reversible solid state hydrogen storage in $NaAlH_4$ by Bogdanović and Schwickardi [3] (although reversibility was already demonstrated in 1974 by Dymova et al. for reactions in the melt [4]). Since then, $NaAlH_4$ has received massive attention focusing on improved doping procedures, screening of catalytic additives, maximizing the reversible capacity, and on obtaining a comprehension of the catalytic effect of Ti (see Refs. [5–10] and references therein).

As a hydrogen storage medium $LiAlH_4$ has not received the same attention as $NaAlH_4$, although several studies, both theoretical and experimental, have revealed important details about its thermal decomposition behaviour, thermodynamic stability, crystal structure, and the effect of ball milling and catalytic doping on its decomposition behaviour (see Refs. [11–31]).

Hydrogen is generally expected to desorb from $LiAlH_4$ in a three-step decomposition, I–III [14–16], although some controversy about the details of the mechanism exists [17,18].

$$LiAlH_4 \rightarrow \tfrac{1}{3}Li_3AlH_6 + \tfrac{2}{3}Al + H_2, \quad (1)$$

$$\tfrac{1}{3}Li_3AlH_6 \rightarrow LiH + \tfrac{1}{3}Al + \tfrac{1}{2}H_2, \quad (2)$$

$$LiH \rightarrow Li + \tfrac{1}{2}H_2. \quad (3)$$

Reactions I, II, and III proceed with a theoretical hydrogen release of 5.3, 2.6, and 2.6 wt%, respectively. However, due

*Corresponding author. Materials Research Department, Risø National Laboratory, DK-4000 Roskilde, Denmark. Fax: +45 4677 5758.
E-mail address: andr1976@gmail.com (A. Andreasen).
[1]Present address: MAN B&W Diesel A/S, Basic Research and Emission, Teglholmsgade 41, DK-2450 Copenhagen SV, Denmark.

0022-4596/$ - see front matter © 2005 Elsevier Inc. All rights reserved.
doi:10.1016/j.jssc.2005.09.027

to the thermodynamic stability of LiH, i.e. high decomposition temperature, only 7.9 wt% H_2 is considered accessible for practical applications.

The kinetic parameters of reactions I and II have only been evaluated to a limited extent [13,31]. These investigations suffer either from unclear separation of parameters from reactions I and II [13] or limitations to reaction I only [31]. This serves as a main motivation for studying the dehydrogenation kinetics of both steps I and II for pure $LiAlH_4$. Furthermore, no systematic investigations of the influence of ball milling, application of different milling times, on kinetics have been reported. These investigations are essential in order to obtain a reliable reference for evaluation of the kinetic effects of doping with catalytic additives in combination with ball milling.

In this paper, we investigate the kinetics of direct dehydrogenation of solid $LiAlH_4$ by carrying out isothermal experiments below the melting point of $LiAlH_4$. In order to extract parameters for both reactions I and II a kinetic model, which takes both reactions into account is formulated, and kinetic parameters are found by fitting to experimental data. Finally, we investigate the effect of altering ball-milling times on the dehydrogenation kinetics of both reactions I and II. Using X-ray powder diffraction it is possible to obtain corresponding crystallite sizes from line broadening and relate this to the observed kinetic effect.

2. Experimental

Lithium aluminium hydride, $LiAlH_4$ (purity 95% min., typically 97%), was obtained in powder form from Alfa Aesar (Johnson Matthey). All materials handling was carried in an argon filled glove box in the presence of a drying agent.

X-ray powder diffraction (XRPD) was performed with a Bragg-Brantano STOE diffractometer (50 kV, 300 mA, Cu$K_{\alpha 12}$ radiation with $\bar{\lambda} = 1.5418$ Å). Powdered samples were pressed into 13 mm diameter pellets with a height of a few millimetres using a pressing tool placed in the glove box. While still in the glove box, a pellet was placed in a specially designed air-tight sample holder with an aluminium foil X-ray window. All observed peaks in the XRPD pattern of the as-received $LiAlH_4$ except for one could be indexed as belonging to a monoclinic unit cell ($P2_1/c$) with unit cell parameters $a = 4.83$ Å, $b = 7.83$ Å, $c = 7.92$ Å, and $\beta = 112.3^\circ$ in agreement with previous observations of the crystal structure of $LiAlH_4/LiAlD_4$ [28,29]. The unexplained peak around $2\theta = 35^\circ$ corresponds well with the strongest reflection of LiCl, suggesting that LiCl is present as an impurity as also suggested by Hauback et al. [16,29]. LiCl might originate from the preparation procedure [25]. We find no other impurities, e.g. hydroxides [16] or oxides [30], suggesting that these are either absent or in an X-ray amorphous state.

Ball milling was utilized with a Retsch PM 100 planetary ball mill using a Wolfram Carbide (WC) vial with a WC-coated aluminium lid sealed with a rubber O-ring. Three WC balls with a diameter of ~20 mm and a weight of ~60 g each were used for all ball-milling experiments. Typically 4–5 g of sample was ball milled giving a ball-to-sample mass ratio of 36–45:1.

Isothermal dehydrogenation of $LiAlH_4$ was studied using a Sartorius 4406 high-pressure balancing unit described in detail elsewhere [32]. In the glove box, typically 60–80 mg of sample was loaded in a stainless-steel crucible with a weight of ~800 mg. The crucible was placed in a sealed plastic bottle in order to protect it against air exposure during transportation from the glove box to the instrument. However, a short period of air exposure (<2 min.) could not be avoided when the sample was transferred from the plastic bottle. An empty stainless-steel crucible was used as a reference. Before the experiment was initiated, the system was evacuated to 10^{-1} mbar and refilled with Helium N47 purity from Air Liquide to 1 bar. This was repeated three times in order to keep the level of impurities (moisture and oxygen) at a tolerable level during the experiment. The sample was heated to the desired isothermal operating temperature at a heating rate of 10 °C/min. The gravimetric hydrogen release from the sample was determined on-line.

3. Results and discussion

3.1. Dehydrogenation kinetics of as-received $LiAlH_4$

In order to investigate the direct solid state decomposition of pure $LiAlH_4$ [15,17], isothermal experiments at different temperatures have been carried out well below the melting point of $LiAlH_4$. The results are shown in Fig. 1(A). As seen in the figure, increasing the temperature increases the rate of hydrogen release as would be expected for a thermally activated process.

Except for the lowest applied temperature, it is evident from the kink in the dehydrogenation curves at a hydrogen release of ~4.5 wt% that the decomposition of $LiAlH_4$ into LiH, Al and H_2 is indeed a two-step mechanism. The position of this transition is somewhat lower than expected from the theoretical hydrogen release. The maximally observed hydrogen release of ~6.7 wt% is also slightly lower than the theoretical limit even when correcting the observed hydrogen release with the purity of the sample. XRPD of the dehydrogenated samples (see list of reflections with assigned phases in Table 1) reveal that some Li_3AlH_6 (and possible also $LiAlH_4$) is left after dehydrogenation in agreement with observations of Andrei et al. [33]. Thus incomplete dehydrogenation of Li_3AlH_6 offers, at least partially, an explanation for this difference.

Modelling the kinetics of hydrogenation/dehydrogenation is essential in order to gain a detailed comprehension of the underlying physics and to identify rate-limiting step(s) of the overall process. This type of kinetic modelling has recently been performed in the case of $NaAlH_4$ [35–37].

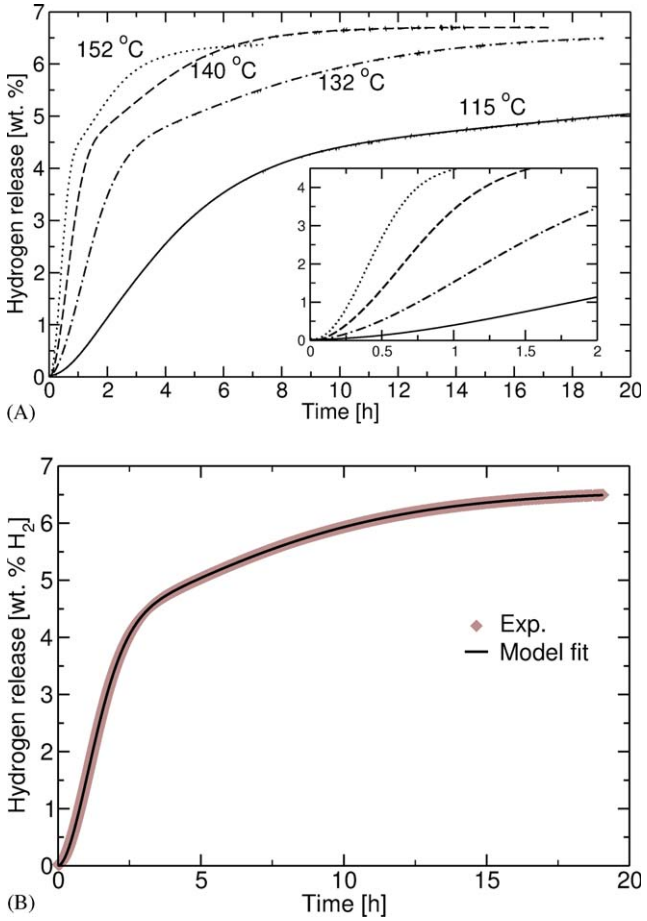

Fig. 1. (A) Isothermal dehydrogenation of as-received $LiAlH_4$ investigated in a high-pressure balance. (B) Fit of Eq. (4) to isothermal dehydrogenation data at $T = 132\,^{\circ}C$.

Table 1
Observed reflections in XRPD of a pellet pressed from the dehydrogenation product of all four as-received samples

2θ (deg)	d (Å)	I/I_{max} (%)	Phase
21.99	4.0393	1.46	Li_3AlH_6
22.55	3.9492	1.53	Li_3AlH_6
29.68	3.0071	0.96	$LiAlH_4$
30.12	2.9646	1.74	$LiAlH_4$
30.42	2.9358	1.56	$LiAlH_4$
31.70	2.8202	1.18	Li_3AlH_6
34.92	2.5673	1.47	Li_3AlH_6
38.54	2.3344	100	Al/LiH
39.97	2.2539	0.74	Li_3AlH_6
44.79	2.0219	43.93	Al/LiH

Phases of Li_3AlH_6 and $LiAlH_4$ have been assigned according to Refs. [28,34].

In order to model the isothermal dehydrogenation curves in Fig. 1(A), a model with the ability to account for both decomposition reactions should be chosen. A standard two-step kinetic expression of the following form provides a good fit to the experimental data

$$W_{tot}(t) = W_1(1 - \exp(-(k_1 t)^{\eta_1})) + W_2(1 - \exp(-(k_2 t)^{\eta_2})), \quad (4)$$

where W_{tot} is the total hydrogen release at time t, W_1 and W_2 are the release of hydrogen from reactions I and II, respectively; k_1 and k_2, and η_1 and η_2 are exponents for reactions I and II, respectively. Except for the included exponents in Eq. (4) the model is similar to the one applied by Kiyobayashi et al. in order to model dehydrogenation of $NaAlH_4$ [35]. Since only dehydrogenation is considered—and the fact that dehydrogenation is performed at constant pressure—pressure-dependent terms, as proposed by Luo and Gross [37] are ignored.

The kinetic expression is fitted to the isothermal experimental data using a Levenberg–Marquandt least-squares algorithm. A sample fit of Eq. (4) to the isothermal dehydrogenation curve at 132 °C is shown in Fig. 1(B). As seen in the figure, the model provides an excellent description of the dehydrogenation kinetics.

All extracted fitting parameters, and apparent activation energies and prefactors as determined from an Arrhenius analysis are summarized in Table 2, including χ^2 goodness-of-fit values.[1]

Early studies on the kinetics of the isothermal decomposition of $LiAlH_4$ by McCarthy et al. [13] revealed an apparent activation energy of reaction I to be ~100 kJ/mol, although it is unclear to which degree the fitted data had been influenced by reaction II. Recent studies by Blanchard et al. [31] shows a value of 102 kJ/mol for reaction I. The value of the apparent activation energy determined in this study is slightly lower (82 kJ/mol), but nevertheless in good agreement with the previous studies. McCarthy et al. [13] also reported an apparent activation energy of reaction II from constant heating rate experiments of ~100 kJ/mol which is also in good agreement with the reported value of 90 kJ/mol in this work. While the work of Blanchard et al. [31] and McCarthy et al. [13] have been limited to treating one reaction at a time, the formulation of a two-step kinetics model has allowed simultaneous extraction of kinetic parameters of both reactions I and II from a single experiment.

3.2. Kinetic effect of ball milling

In order to investigate the effect of ball-milling $LiAlH_4$ on the dehydrogenation kinetics, the as-received powder has been ball milled for different periods of time and milling intensities. These samples have been subject to both

[1] χ^2 goodness-of-fit calculated for each temperature by

$$\chi^2 = \frac{1}{N}\sum_{i=1}^{N}\left(\frac{(W_{obs}(i) - W_{model}(i))^2}{W_{model}(i)}\right),$$

where N is the total number of observations during an isothermal experiment, W_{obs} is the experimentally observed hydrogen release, and W_{model} is the calculated hydrogen release using Eq. (4).

Table 2
Kinetic parameters obtained from fitting isothermal measurements of the direct decomposition of as-received $LiAlH_4$

T (°C)	W_1 (wt% H_2)	W_2 (wt% H_2)	k_1 (h^{-1})	k_2 (h^{-1})	η_1 (dimensionless)	η_2 (dimensionless)	χ^2
115	4.28	1.56	0.229	0.040	1.53	1.95	0.0133
132	4.11	2.44	0.624	0.123	1.80	1.51	0.0030
140	4.25	2.44	1.191	0.235	1.99	1.71	0.0007
152	4.02	2.32	1.996	0.442	2.22	1.74	0.0302
A (h^{-1})			2.3×10^{10}	4.9×10^{10}			
E_A (kJ/mol)			82 ± 4	90 ± 4			

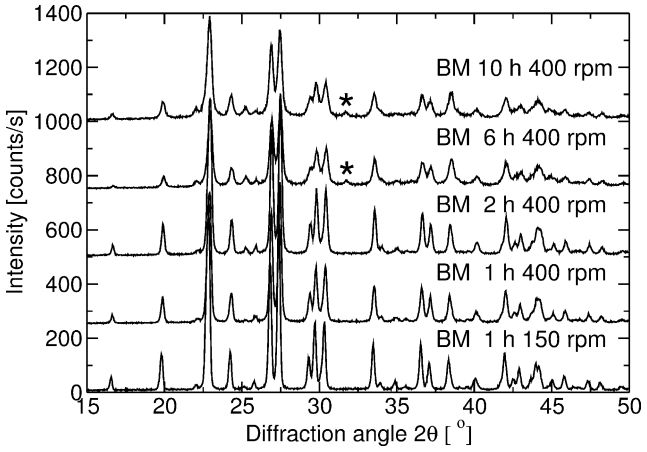

Fig. 2. XRPD of as-received $LiAlH_4$, $LiAlH_4$ ball milled for 1 h at 150 rpm, and $LiAlH_4$ ball milled for 1 h at 400 rpm.

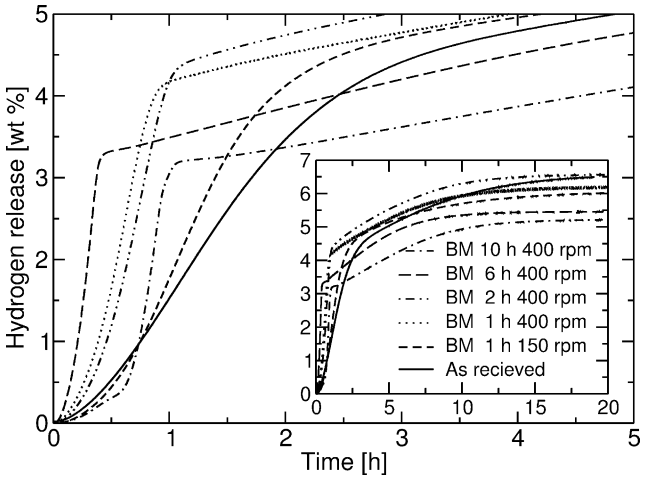

Fig. 3. Isothermal dehydrogenation curves for ball-milled samples. The isothermal temperature is ~130 °C. Dehydrogenation curve for un-milled as-received $LiAlH_4$ at 132 °C is included for comparison.

XRPD analysis and isothermal measurements of the dehydrogenation process.

XRPD patterns of all the ball milled samples are shown in Fig. 2. Generally, the reflections become broader and lose intensity as a function of milling time/intensity suggesting that the average coherence length (crystallite size) is reduced upon milling. After 6 h of milling an additional reflection (marked with an asterisk) appears around $2\theta = 31.7°$. This feature could originate from either the (2 2 0) reflection of monoclinic [34] Li_3AlH_6 or the (2 0 −1) reflection of rhombohedral Li_3AlH_6 [20], suggesting a partial decomposition of $LiAlH_4$. In fact, after 2 h of milling, the sample changed colour from white/greyish to light grey indicating that a solid state reaction had taken place. On the other hand, apparently no crystalline metallic aluminium is formed suggesting that if any formation of Li_3AlH_6 has taken place the resulting aluminium is in an X-ray amorphous phase. Partial decomposition of $LiAlH_4$ into Li_3AlH_6 can be explained in terms of a higher thermodynamic stability of Li_3AlH_6 compared to $LiAlH_4$ [11,15,19–22]. Although the ball-milling vial used in this work was carefully cleaned, the presence of small amounts of impurities that may act as a catalyst [26] cannot be completely ruled out. However, we consider this as unlikely. On the other hand, we noticed that the vial heated up slightly during milling, most pronounced for the longer milling times. Thus, the potential decomposition of $LiAlH_4$ may be thermally mediated.

The effect of ball milling on the dehydrogenation kinetics is visualized by isothermal dehydrogenation curves for all ball-milled samples in Fig. 3. It was intended to apply the same isothermal temperature to all dehydrogenation experiments for the ball-milled samples. Though, in practice, an inter-sample temperature variance of a few degrees around 130 °C was observed, which is expected to be within experimental uncertainty. The dehydrogenation curve for as-received $LiAlH_4$ at 132 °C is included in Fig. 3 as a reference.

From the dehydrogenation curves in Fig. 3 it is observed that ball milling effectively leads to faster kinetics for reaction I (first and steepest part of the curves up to 3–4.5 wt%), while reaction II seems to be more insensitive to the ball-milling. Applying longer ball milling times, the smooth transition between reactions I and II as observed in the un-milled sample become more abrupt. The initial rate of dehydrogenation for the sample ball milled for 10 h seems to deviate somewhat from the others. This is due to the fact that dehydrogenation initiated during the heating

Table 3
Kinetic parameters obtained from fitting isothermal measurements of the direct decomposition of ball-milled $LiAlH_4$

Time (h)	Intensity (rpm)	W_1 (wt% H_2)	W_2 (wt% H_2)	k_1 (h^{-1})	k_2 (h^{-1})	η_1 (dimensionless)	η_2 (dimensionless)	χ^2
1	150	3.85	2.17	0.751	0.180	2.48	1.18	0.0002
1	400	4.12	2.07	1.567	0.168	2.78	1.41	0.0047
2	400	3.57	3.26	1.305	0.190	3.66	0.80	0.0020
6	400	3.39	2.04	3.272	0.216	2.95	1.60	0.0095
10	400	2.81	1.97	3.817	0.163	2.26	1.63	0.0113

period. It is also observed from Fig. 3 that longer ball-milling times results in reduced hydrogen release mainly from $LiAlH_4$.

In order to quantify the effect of ball milling on the dehydrogenation kinetics of $LiAlH_4$, kinetic parameters are extracted from the dehydrogenation curves by fitting Eq. (4) to the experimental dehydrogenation curves of the ball-milled samples; the results are summarized in Table 3. In order to fit the dehydrogenation curve of the sample ball milled for 10 h it was necessary to exclude the first part of the curve corresponding to the non-isothermal hydrogen release from the fitting procedure. As seen from the fitted parameters in Table 3 the faster kinetics of reaction I seen in Fig. 3 is confirmed quantitatively. It is interesting to see that ball milling has virtually no effect on the rate constant of reaction II.

From Table 3 it is clearly observed that the parameter W_1 decreases as a function of milling time, especially for the longest periods of milling. This suggests some partial decomposition of $LiAlH_4$ during milling as discussed previously, and also in agreement with Fig. 3. This requires a careful application of the kinetic model. However, we find no reasons to believe that the fitting results are biased by the initial presence of Li_3AlH_6 in the ball-milled samples. First, the decomposition of Li_3AlH_6 is slow compared to the decomposition of $LiAlH_4$ as visualized by both Figs. 1(A) and 3. This is even more pronounced for the samples ball milled for the longest times. According to Fig. 3, the dehydrogenation of $LiAlH_4$ becomes so fast for the longest periods of milling, that an induction period in the decomposition of Li_3AlH_6 is revealed. Thus for the samples containing Li_3AlH_6 from the beginning, effectively no decomposition of Li_3AlH_6 takes place before all $LiAlH_4$ is completely transformed into Li_3AlH_6. Second, the fitting parameter W_2 shown in Table 3 is more or less constant even despite the initial presence of Li_3AlH_6. This is a natural consequence of the first point and it gives confidence in the fact that the two dehydrogenation steps described by the model are treated as separate reactions without any intermixing of kinetic parameters, i.e. the kinetic parameters of step I are independent of the kinetic parameters of step II and vice versa.

3.3. Diffusion limited kinetics?

In order to investigate a possible correlation between crystallite size and rate constants we have extracted crystallite sizes of the ball-milled samples before dehydrogenation including the as-received sample by applying the Scherrer equation

$$\beta = \frac{\lambda}{B\cos\theta}, \tag{5}$$

where β is the crystallite size, λ is the X-ray wavelength and B is the FWHM (corrected for instrumental broadening, which is assumed to be 0.10°). In order to get a reliable picture of the average crystallite size instead of an average coherence length in certain crystallographic directions, the average line broadening of several reflections up to 35° in 2θ have been used.

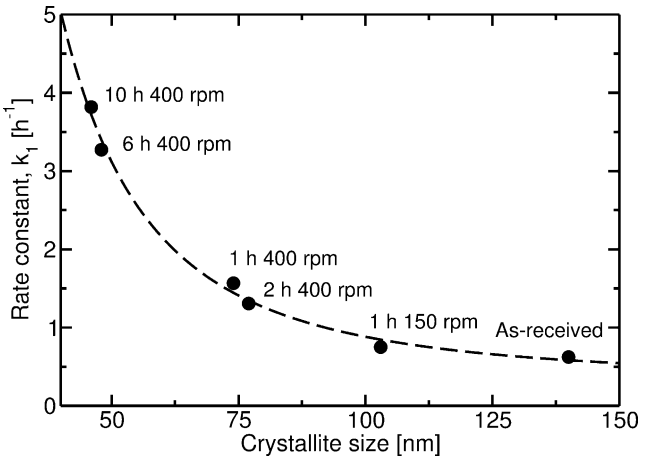

Fig. 4. Rate constants for reaction I as a function of crystallite size obtained from XRPD line broadening.

Fig. 4 shows the rate constants as a function of crystallite size. Fitting the data to a power-law yields an excellent fit (dashed line) with an $1/\beta^{2.3}$ dependence. The strong dependence of k_1 on crystallite size may suggest a mass transfer process to be limiting the kinetics, e.g. long-range atomic diffusion of Al as proposed by Kiyobayashi et al. [35] and Sandrock et al. [7]. The exact order of the exponent can be used to obtain detailed physical information about the underlying rate-limiting process(es).

In the Nabarro–Herring model [38,39], a $1/\beta^2$ relation corresponds to a process controlled by lattice (intergranular) diffusion as observed for e.g. hydrogen diffusion in $Co_{90}Zr_{10}$ [40], whereas a process controlled by grain boundary diffusion displays a $1/\beta^3$ relation according to Coble [41]; as observed for e.g. hydrogen enhanced

diffusional creep in Pd [42]. Considering Fig. 4 displays a $1/\beta^{\sim 2}$ relation, reaction I is likely limited by a lattice diffusional process, although grain boundary diffusion cannot be excluded.

The fact that k_2 is more or less insensitive to the large variations in crystallite size indicates that reaction II, in contrast to reaction I, is not limited by mass transfer. Instead, the intrinsic kinetics seems to be limiting at the relatively low temperature applied. Previous DTA results [26] show that the kinetics of reaction II at elevated temperatures is indeed improved by ball milling as seen by a lowering of the decomposition temperature from ~250 to 225 °C after ball milling for only 10 min. This suggests that at the elevated temperatures in the DTA experiment, the intrinsic kinetics is improved sufficiently in order *not* to be rate limiting for the overall kinetics. Instead, the crystallite size seems to become important. However, for practical applications the temperature cannot be increased above 200 °C in order to obtain improved kinetics. Thus, ball milling alone is not sufficient to improve the kinetics of reaction II. This example very clearly illustrates the need for a suitable catalytic additive, not only to the make reaction I + II reversible [21] but also to improve the kinetics—especially of reaction II.

3.4. Influence on oxygen contamination on kinetics

Although no oxygen contamination is observed in any of the XRPD results shown in this study, it seems unquestionable that the samples contain a certain amount of oxides. This is supported by the studies of Andrei et al. [30] in which aluminium oxide was detected by EELS, even though the samples have been carefully transferred from the glove box to the instrument in a special vacuum transfer device including a removable glove bag mounted on the instrument.

The results of Andrei et al. [30] also indicated that the found aluminium oxide forms a thin layer on the particles. Hence, dehydrogenation may potentially be limited by hydrogen diffusion through the surface oxide. Although, we find this to be highly unlikely. Mainly, because even for the ball-milled samples the main weight fraction of samples belong to particles of several microns (as found by additional SEM experiments) making the determined crystallite sizes a "bulk" quantity. Thus, if diffusion through the surface oxide was rate limiting, one would not expect such a strong correlation between rate and crystallite size. Furthermore, the similarity of apparent activation energies of both reactions I and II with previous studies [13,31] despite differences in sample treatment seems to support this hypothesis.

4. Conclusion

We have investigated the dehydrogenation kinetics of as-received and ball-milled $LiAlH_4$. Isothermal experiments reveal apparent activation energies of 82 and 90 kJ/mol for dehydrogenation of $LiAlH_4$ to Li_3AlH_6 (reaction I) and the subsequent dehydrogenation of Li_3AlH_6 to LiH (reaction II), respectively.

Investigations of ball-milling $LiAlH_4$ for different periods of time and subsequent kinetic investigations at isothermal conditions at ~130 °C clearly show improved kinetics of the dehydrogenation reaction I as a function of milling time, whereas reaction II seems more or less insensitive to the ball-milling process. Detailed kinetic fitting allowing extraction of rate constants for both reactions I and II shows a clear correlation between the rate constant of reaction I and crystallite size determined from XRPD line broadening with higher rate constant corresponding to smaller crystallite sizes (longer ball-milling times). In contrast, the rate constant of reaction II is more or less unchanged despite the drastic reduction in crystallite size of $LiAlH_4$ going from 140 to 46 nm. This suggests reaction I is limited by mass transfer, whereas reaction II is limited by the intrinsic kinetics. Thus a suitable catalyst is needed in order to improve the kinetics, not only for the reversibility of reactions I and II, but certainly also the kinetics of reaction II at temperatures suitable for practical applications.

Acknowledgements

This work has received financial support from The Danish Technical Research Council through the Center of Excellence *Towards a hydrogen-based society*.

References

[1] L. Schlapbach, A. Züttel, Nature 414 (2001) 353–358.
[2] Basic research needs for the hydrogen economy, Technical Report, Argonne National Laboratory, Argonne, IL 60439, USA, 2003.
[3] B. Bogdanović, M. Schwickardi, J. Alloys Compd. 253–254 (1997) 1–9.
[4] T.N. Dymova, Y.M. Dergachev, V.A. Sokolov, N.A. Grechanaya, Dokl. Akad. Nauk. SSSR 215 (1974) 1369–1372.
[5] D.L. Anton, J. Alloys Compd. 356 (2003) 400–404.
[6] K.J. Gross, E.H. Majzoub, S.W. Spangler, J. Alloys Compd. 356–357 (2003) 423–428.
[7] G. Sandrock, K. Gross, G. Thomas, C. Jensen, D. Meeker, S. Takara, J. Alloys Compd. 330–332 (2002) 686–701.
[8] A. Leon, O. Kirchner, J. Rothe, M. Fichtner, J. Phys. Chem. B 108 (42) (2004) 16372–16376.
[9] M. Felderhoff, K. Klementiev, W. Grunert, B. Spliethoff, B. Tesche, J.M.B. von Colbe, B. Bogdanović, M. Hartel, A. Pommerin, F. Schuth, C. Weidenthaler, Phys. Chem. Chem. Phys. 6 (17) (2004) 4369–4374.
[10] H.W. Brinks, C.M. Jensen, S.S. Srinivasan, B.C. Hauback, D. Blanchard, K. Murphy, J. Alloys Compd. 376 (2004) 215–221.
[11] P. Claudy, B. Bonnetot, J.M. Létoffé, G. Turck, Thermochim. Acta 27 (1978) 213–221.
[12] J. Block, A.P. Gray, Inorg. Chem. 4 (1965) 304–305.
[13] M. McCarthy Jr., J.N. Maycook, V.R. Pai Verneker, J. Phys. Chem. 72 (1968) 4009–4014.
[14] J.A. Dilts, E.C. Ashby, Inorg. Chem. 11 (6) (1972) 1230–1236.
[15] T.N. Dymova, D.P. Aleksandrov, V.N. Konoplev, T.A. Silina, A.S. Sizareva, Russ. J. Coord. Chem. 20 (4) (1994) 279–285.

[16] D. Blanchard, H.W. Brinks, B.C. Hauback, P. Norby, Mater. Sci. Eng. B 108 (2004) 54–59.
[17] J.W. Wiench, V.P. Balema, V.K. Pecharsky, M. Pruski, J. Solid State Chem. 177 (2004) 648–653.
[18] V.P. Balema, L. Balema, Phys. Chem. Chem. Phys. 7 (6) (2005) 1310–1314.
[19] M.B. Smith, G.E. Bass Jr., J. Chem. Eng. Data 8 (3) (1963) 342–346.
[20] O.M. Løvvik, S.M. Opalka, H.W. Brinks, B.C. Hauback, Phys. Rev. B 69 (2004) 134117.
[21] J. Chen, N. Kuriyama, Q. Xu, H.T. Takeshita, T. Sakai, J. Phys. Chem. B 105 (2001) 11214–11220.
[22] S.C. Chung, H. Morioka, J. Alloys Compd. 372 (2004) 92–96.
[23] V.P. Balema, K.W. Dennis, V.K. Pecharsky, Chem. Comm. (17) (2000) 1665–1666.
[24] L. Zaluski, A. Zaluska, J.O. Ström-Olsen, J. Alloys Compd. 290 (1999) 71–78.
[25] E. Wiberg, E. Amberger, Hydrides of the Elements of Main Groups I–IV, Elsevier, Amsterdam, 1971.
[26] V.P. Balema, V.K. Pecharsky, K.W. Dennis, J. Alloys Compd. 313 (2000) 69–74.
[27] V.P. Balema, J.W. Wiench, K.W. Dennis, M. Pruski, V.K. Pecharsky, J. Alloys Compd. 329 (2001) 108–114.
[28] N. Sklar, B. Post, Inorg. Chem. 6 (1967) 669.
[29] B.C. Hauback, H. Brinks, H.W. Fjellvåg, J. Alloys. Compd. 346 (2002) 184–189.
[30] C.M. Andrei, J.C. Walmsley, H.W. Brinks, R. Holmestad, B.C. Blanchard, D. Hauback, G.A. Botton, J. Phys. Chem. B 109 (2004) 4350–4356.
[31] D. Blanchard, H.W. Brinks, B.C. Hauback, P. Norby, J. Muller, J. Alloys Compd. (2005) doi:10.1016/j.jallcom.2005.01.126.
[32] A.S. Pedersen, J. Kjøller, B. Larsen, B. Vigeholm, Int. J. Hydrogen Energy 8 (3) (1983) 205–211.
[33] C.M. Andrei, J. Walmsley, D. Blanchard, H.W. Brinks, R. Holmestad, B.C. Hauback, J. Alloys. Compd. 395 (2005) 307–312.
[34] J. Mayet, J. Tranchan, Bull. Soc. Chim. Fr. (2) (1973) 510.
[35] T. Kiyobayashi, S.S. Srinivasan, D. Sun, C.M. Jensen, J. Phys. Chem. A 107 (39) (2003) 7671–7674.
[36] R.T. Walters, J.H. Scogin, J. Alloys Compd. 379 (2004) 135–142.
[37] W. Luo, K.J. Gross, J. Alloys Compd. 385 (2004) 224–231.
[38] C. Herring, J. Appl. Phys. 21 (1950) 437–445.
[39] F.R.N. Nabarro, H.L. de Villiers, The Physics of Creep, Taylor & Francis, 1995.
[40] M. Hirsher, J. Mössinger, H. Kronmüller, NanoStructured Mater. 6 (1995) 635–638.
[41] R.L. Coble, J. Appl. Phys. 34 (1963) 1679–1682.
[42] Z.R. Xu, R.B. McLellan, Acta Mater. 46 (1998) 4543–4547.